

# Theoretical Investigation of Cathodes in High Power Arcjets\*

K. D. Goodfellow<sup>†</sup>  
*Jet Propulsion Laboratory*  
*California Institute of Technology*  
*Pasadena, California*

## Abstract

Cathode erosion is one of the life limiting mechanisms in several classes of electric thrusters. Since cathode erosion depends strongly on the cathode temperature, a quantitative understanding of the effects of cathode operation on the cathode temperature is required. Improvements to the near-cathode plasma including the addition of double ions, multiple gas types, and a model of equilibrium ionization/recombination within the ionization region are also included. A quasi-two-dimensional model approximation has been added to a thermal model allowing the use of arc attachment areas smaller than the total tip area. This addition allows the attachment area to be changed so that the effect of operating conditions (pressure, gas type, geometry, etc. ) at a constant total current can now be compared. This addition provides a new stable low temperature solution that agrees well with the experimental data. Excellent agreement between the new model and high-power long-duration ammonia arcjet data has been achieved. Furthermore, post-test analysis of these cathodes indicates that portions of the cathode tips were molten during operation. Concurrently, the model predicts temperatures near the melting point of tungsten for attachment areas consistent with the areas observed in the experiments.

## Introduction

One of the major issues for the use of electric propulsion thrusters is lifetime. Mission analyses estimate that, for electric propulsion to be a viable option, thruster lifetimes must be of the order of 1000 to 15,000 hours. Cathode erosion, one of the primary life-limiting mechanisms, has been shown to depend strongly on the cathode temperature [1]. Therefore, part of this study is intended to **provide a means of predicting** the cathode temperature for various thruster operating conditions. The combined plasma and thermal models also provide the appropriate boundary conditions at the cathode surface for models of the operating characteristics of the thruster. For example, the current

---

\*Copyright © 1991 American Institute of Aeronautics and Astronautics, Inc., all rights reserved.

<sup>†</sup>Member of the Technical Staff, Advanced Propulsion Technology Group

contours within the magnetoplasmadynamic (MPD) thruster cannot be specified independently of the cathode temperature distribution because the majority of the current is from thermionic emission. Since the cathode model boundary conditions also depend on the characteristics of the main plasma, the two models must be ultimately coupled to obtain an overall model of the cathode region of the thruster.

Several different approaches have been taken in the past to characterize the nature of the hot-cathode arc physics [2,3,4,5] while others have focussed on the thermal model alone [6,7,8]. Past works have focussed primarily on one or the other of these models, but some combined models have been presented [9,10,11,12]. That is, the plasma model provides the heat loads (boundary conditions) for the thermal model, and the thermal model provides the surface temperature which strongly affects the plasma near the cathode through thermionic emission.

The thermal characteristics of cathodes in high-current gas discharges are being investigated in a dedicated cathode test facility at the Jet Propulsion Laboratory (JPL). Axial temperature distributions and near-cathode plasma properties are being measured for various cathode configurations as a function of current level, ambient gas pressure and flow rate. The objective of these experiments is to provide a database of measurements for comparison with theoretical predictions based on one-dimensional and two-dimensional heat transfer models of the solid cathode with radiation, convection and plasma sheath (arc attachment) boundary conditions. In this paper, improvements to both the thermal and plasma models will be presented and compared with high-power ammonia arcjet data. A companion paper, Ref. [13], contains additional experimental data and model comparisons for low-pressure high-current discharges.

## Cathode Model

The cathode model consists of two parts, namely a near-cathode plasma model and a thermal model of the cathode. The near-cathode plasma model connects the properties of the main plasma with the cathode. Specifically, given the plasma properties within a mean-free-path of the surface, the near-cathode model predicts the heat flux and current density to the cathode surface. With these boundary conditions and the traditional thermal transport mechanisms, the thermal model can predict the temperature distribution within the cathode. Because of the interdependency of the two models, they must be solved simultaneously.

### Near-Cathode Plasma Model

An illustration of the near-cathode plasma is shown in Fig. (1). The Debye length, mean free path, and thermal, concentration and momentum boundary layers are represented by  $L_D$ ,  $L_{ei}$  and  $L_{T,C,M}$  respectively. For this study, only the surface, sheath, presheath and ionization regions are modeled. In the main body of the plasma, the current is predominantly carried by the electrons, while in the sheath region the ion current may dominate. To match these regions an ionization region (which produces the required number of ions for the sheath region) is required between the sheath and the main plasma body. Similarly, a recombination region exists at the cathode surface to produce a transition to pure electron conduction in the solid. At the surface, ions are also converted to neutrals, which then return to the plasma. A complete description of each region

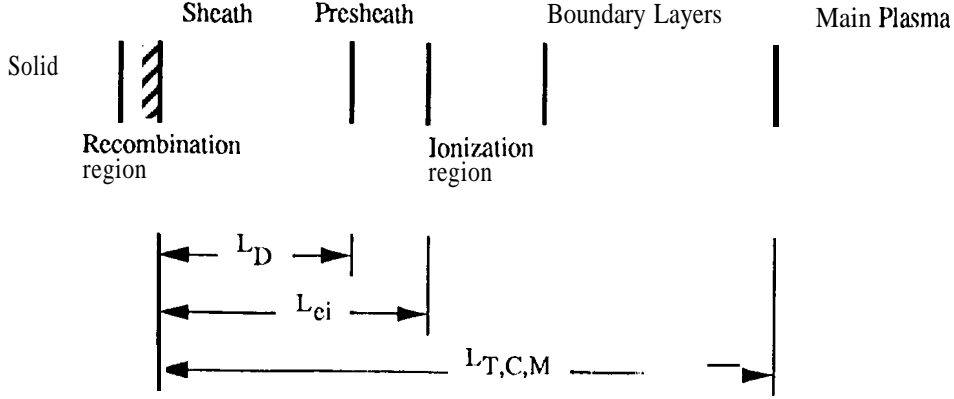


Figure 1: Near-cathode plasma regions.

model, the overall near-cathode plasma model and sample solutions are given in Refs.[11], [12] and [14].

In general the cathode surface is characterized by the material, the surface finish and the temperature. For this model, the recombination region is assumed to be infinitesimally thin and is considered as a surface effect. Incident particles from the sheath heat the surface while emitted particles cool the surface. The energy balance at the surface balances the energy deposited and removed by the particles with heat conduction into the solid, and radiative, convective and mass (surface erosion) transport to the surroundings. The surface heat flux is the net of the energy deposited from the incident ions and plasma electrons, and the energy removed by the thermionic electrons. The incident ions are recombined and reemitted as neutrals. The net heat flux to the surface due to the plasma is given by

$$\begin{aligned}
 q_{\text{tot}} &= q_{i,1} + q_{ii,1} - q_{n,1} + q_{i,2} + q_{ii,2} - q_{n,2} - q_b + q_e \\
 &= \sum_{s=1}^2 \left[ \frac{j_{i,s}}{e} (eV_c + eV_B + \epsilon_{i,s} - \phi_{\text{eff}}) + \frac{j_{ii,s}}{2e} (2eV_c + eV_B + \epsilon_{ii,s} - 2\phi_{\text{eff}}) \right] \\
 &\quad - \sum_{s=1}^2 [F_{n,c,s} 2kT_c] - \frac{j_b}{e} (\phi_{\text{eff}} + 2kT_c) + \frac{j_e}{e} (\phi_{\text{eff}} + 2kT_e)
 \end{aligned} \tag{1}$$

where Boltzmann's constant is expressed in units of eV/K. Note that there is a typographical error in this equation in Refs. [11] and [12]. The net current is given by

$$j_{\text{tot}} = j_{i,1} + j_{ii,1} + j_{i,2} + j_{ii,2} + j_b - j_e. \tag{2}$$

For high cathode temperatures, thermionic emission is the dominant current conduction mechanism in the near-cathode region [10]. Thermionic emission is described by the empirical Richardson-

$$(7) \quad n \equiv \frac{eV}{kT_e}$$

$$(6) \quad v_{i,s} \equiv \frac{n_{i,s}}{n_{i,o,s}}$$

$$(5) \quad v_{i,2} \equiv \frac{n_{i,o,2}}{n_{i,o,1}} = \frac{X_{i,2}}{X_{i,1}} \beta v_{i,1}$$

$$(4) \quad v_{i,1} \equiv \frac{n_{e,o}}{n_{i,o,1}} = \frac{(1 + 2v_{i,1}) + \frac{X_{i,1}}{X_{i,2}} \beta (1 + 2v_{i,2})}{1 + \int \beta (n_e + E_{b0})^{-1/2}}$$

the remaining normalized variables are given in Eq. (7) through Eq. (10). Expressions for the normalized ion number densities are given in Eq. (4) through Eq. (6) and Poisson charge equation is used to describe the electric field and the electric potential.

flux of the high energy electrons constitutes the plasma electron current. The one-dimensional and those with insufficient energy that are repelled back to the main plasma. The corresponding sufficient kinetic energy to overcome the sheath retarding potential and reach the cathode surface electrons are assumed to be Maxwellian. These electrons fall into two classes, namely those with singly-charged ions would have to maintain charge neutrality at the sheath edge. The plasma charged ions have twice the charge and hence twice the acceleration, their number density is also half the minimum ion energy required for the correct electrostatic solution [17]. Although the doubly-ion mass. A simple proof of this is to consider a sheath with only doubly-charged ions and calculate minimum ion energy is the same for both singly- and doubly-charged ions, and is independent of the Bohm minimum energy which is represented as the Bohm potential,  $V_B$ . The Bohm minimum energy [16]. All of the ions here are assumed to enter the sheath with energies equal to or greater than the Bohm minimum energy to occur, the ions must enter the sheath with energies equal to or greater than

The current data base includes the noble gases, hydrogen, nitrogen and lithium. propellants such ammonia or hydrazine. The gases are assumed to be monatomic and nonreacting. is the ability to use two different gas types. This allows the model to simulate discharges with ions may be significant at low pressures for high current discharges. A second addition to the model added to a previously developed model [11,12,14] because the cathode heating from doubly-charged therefore, magnetic field effects on the particle trajectories are negligible. Doubly-charged ions were plasma [2,4]. Further, the sheath thickness much less than the Larmor radii of the particles, and charged monoenergetic ions for two monatomic gases, and Maxwellian electrons originating in the species are considered, namely monoenergetic thermionic (or beam) electrons, singly- and doubly-potential plus kinetic) since the Debye length is much larger than the collisional mean free paths. Six The sheath region is assumed to contain collisionless particles with constant total energy (po-

$$(3) \quad j_b = A R T_e^2 \exp \left( -\phi_o - \sqrt{\frac{e h c}{4 \pi c_o}} \frac{k T_e}{\phi_o} \right)$$

primarily determined by the characteristics of the sheath region. Dushman relation. In addition, the surface electric field acts to enhance the emission, a phenomenon known as the Schottky effect [15]. The magnitude of the electric field at the cathode surface is

$$\xi \equiv \frac{x}{\sqrt{\frac{\epsilon_0 k T_e}{n_{e,o} e^2}}} \quad (8)$$

$$J_b \equiv \frac{j_b}{e n_{e,o}} \sqrt{\frac{m_e}{2kT_e}} \quad (9)$$

$$F_{bo} \equiv \frac{2kT_e}{kT_e} \quad (10)$$

in addition it has been assumed that the masses of the singly- and doubly-charged ions are equal ( $m_{i,s} = m_{ii,s}$ ). The mole fraction of singly-charge ions for gas type  $s$  is given by  $Y_{i,s}$ , and is discussed in more detail later. Note that  $Y_{i,1}$  will never be exactly zero although it may be very small, That is, there will always be some fraction of singly-charged ions present. The ratio of the partial pressures of the two gas types is given by

$$\beta \equiv \frac{P_2}{P_1} \quad (11)$$

The normalized Bohm minimum ion energy is

$$\eta_B = \frac{eV_B}{kT_e} = \frac{v_{i,1} (1 + 4\nu_{ii,1}) + \nu_{i,2} (1 + 4\nu_{ii,2})}{2 - J_b(\eta_c + F_{bo})^{-3/2}} \quad (12)$$

where  $\nu_{i,1}$  and  $\nu_{i,2}$  are related through Eq.(5) as determined by the technique described in [18,14].

The Poisson equation can then be integrated and solved for the electric field at the cathode surface yields Eq.(13) **which is used to compute the Schottky effect** and completes the description of the thermionic emission current given in Eq. (3) [14].

$$\epsilon_c^2 = \left( \frac{eV_c J_D}{kT_e} \right)^2 = \sum_{s=1}^2 \left[ 4\nu_{i,s} \eta_B \left[ \left( 1 + \frac{\eta_c}{\eta_B} \right)^{1/2} - 1 \right] + 4\nu_{i,s} \nu_{ii,s} \eta_B \left[ \left( 1 + \frac{2\eta_c}{\eta_B} \right)^{1/2} - 1 \right] \right] - 4J_b \left[ (\eta_c + F_{bo})^{1/2} - F_{bo}^{1/2} \right] + 2e^{-\eta_c} - 2 + \epsilon_{sh}^2 \quad (13)$$

The ionization and presheath regions connect the sheath region with the main plasma body [9, 15]. The purpose of the presheath region is to accelerate the ions so that they enter the sheath region with the minimum energy required for a stable sheath (Bohm energy) [16]. For this model the presheath region is combined with the ionization region by requiring that ions leave the ionization region with the Bohm energy. The ionization region generates the required number of ion and electron pairs to match the sheath and main plasma body values. An illustration of the particles entering and leaving the ionization region for a single gas type is shown in Fig. (2). Electrical neutrality is given by

$$n_e = n_{i,1} + 2n_{ii,1} + n_{i,2} + 2n_{ii,2} = n_{e,o} + n_b \quad (14)$$

and the gas ionization for each gas type is given by

$$\dot{n}_{e,s} = \dot{n}_{i,s} + 2\dot{n}_{ii,s} \quad (15)$$

$$\begin{aligned}
 & (F_{0,c,1} + F_{0,c,2}) 2kT_e + \frac{e}{j_b} (eV_c + 2kT_e) - (j_{i,1} + j_{ii,1} + j_{i,2} + j_{ii,2}) \frac{e}{eV_B} \\
 & - \frac{j_e}{j_e} (2kT_e + eV_c) + (j_{i,p,1} + j_{ii,p,1} + j_{i,p,2} + j_{ii,p,2}) \frac{e}{2kT_h} \\
 & - \frac{j_{e,p}}{j_e} 2kT_e + (F_{0,p,1} + F_{0,p,2}) 2kT_h \\
 & - (n_{i,1} \epsilon_{i,1} + n_{ii,1} \epsilon_{ii,1} + n_{i,2} \epsilon_{i,2} + n_{ii,2} \epsilon_{ii,2}) d = 0.
 \end{aligned}
 \tag{22}$$

The energy balance for this region is given by

$$j_{tot} = j_{i,p,1} + j_{ii,p,1} + j_{i,p,2} + j_{ii,p,2} + j_{e,p}.
 \tag{21}$$

The conservation of current density in the free-plasma region is given by

$$-n_{0,s} d = F_{0,c,s} + F_{0,p,s}
 \tag{20}$$

$$e n_{ii,s} d = j_{ii,s} - j_{i,p,s}
 \tag{19}$$

$$e n_{i,s} d = j_{i,s} - j_{i,p,s}
 \tag{18}$$

for recombination at the cathode surface, assuming that the cathode surface is fully accommodating for each gas type. The balance of species fluxes in and out and generation within the ionization region are given by Eqs. 18 through 20 where  $d$  is the thickness of the ionization region.

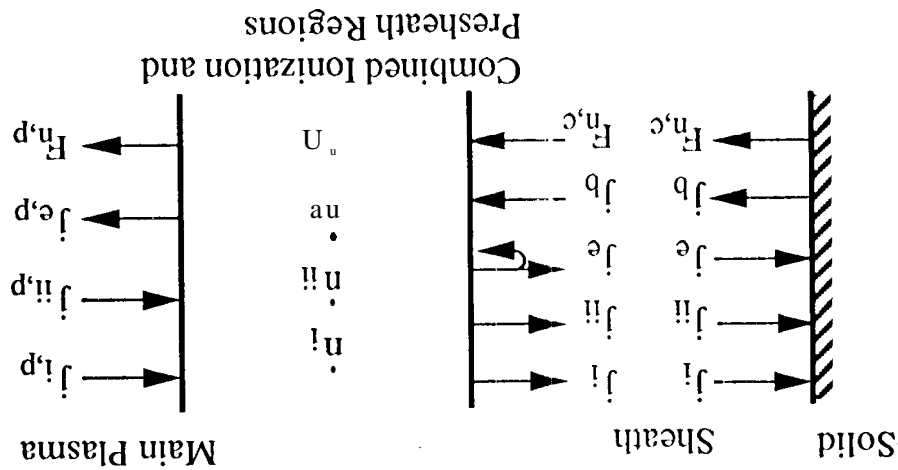
$$e F_{0,c,s} = j_{i,s} + j_{ii,s}
 \tag{17}$$

for the ionization region and by

$$n_{0,s} + n_{i,s} + n_{ii,s} = 0
 \tag{16}$$

Conservation of heavy species generation is given by

Figure 2: Illustration of ionization region.



The predominant terms are the energy added to the region by the thermionic electrons, the energy consumed by ionization, and the energy removed by the ions to the sheath, and the energy removed by the plasma electrons to both the sheath (third term) and the main plasma (fourth term). The relative sizes of the current densities determine which energy removal term dominates. The other terms are significant under special circumstances, for example, at low sheath voltages,

Using Eqs.16 through 20 gives the expression

$$-F_{0,p,s} = j_{i,p,s} + j_{ii,p,s} \quad (23)$$

which is used to write Eq. (22) as a function of current densities. The flux of neutrals from the ionization region to the main plasma is equal to the ion current to the region from the main plasma. It has been assumed that the neutral and ion thermal energies are equal.

For the main plasma, the ion currents can be approximated using the relations

$$j_{i,p,s} = \frac{m_e}{m_{i,s}} j_{tot} \quad (24)$$

$$j_{ii,p,s} = \frac{m_e}{m_{i,s}} \frac{n_{ii,o,s}}{n_{i,o,s}} j_{tot} \quad (25)$$

for a fully ionized plasma [19]. As expected, the ions currents are small compared to the electron current. The ratio of the plasma electron current,  $j_{e,p}$ , to the plasma ion current,  $j_{i,p}$ , can be estimated from their respective electrical conductivities and is of the order of  $m_i/m_e$  [19].

Using these assumptions, Eqs. 2, 17 through 20, and 23 through 25, the energy equation (22) can be written as

$$\begin{aligned} \frac{j_b}{e} (eV_c + 2kT_c) - \sum_{s=1}^2 \left[ \frac{j_{i,s}}{e} (eV_B + \epsilon_{i,s} - 2kT_c) - \frac{j_{ii,s}}{e} (eV_B + \epsilon_{ii,s} - 2kT_c) \right] \\ - \frac{j_e}{e} [2kT_e + eV_c] - \frac{j_{tot}}{e} (2kT_e - C) = 0. \end{aligned} \quad (26)$$

where

$$C = \sum_{s=1}^2 \left[ \frac{m_e}{m_{i,s}} (2kT_e + \epsilon_{i,s}) + \frac{m_e}{m_{i,s}} \frac{n_{ii,s}}{n_{i,s}} (2kT_e + \epsilon_{ii,s}) \right] \quad (27)$$

Using Eq. (21) with the normalization variable given previously, Eq.(26) can be written as

$$\begin{aligned} J_b (\eta_c + E_{bo} - 2 + B) - \sum_{s=1}^2 \left[ \nu_{i,s} \sqrt{\eta_B} \sqrt{\frac{m_e}{m_{i,s}}} (\eta_B + \eta_{i,s} + 2 - E_{bo} - B) \right] \\ - \sum_{s=1}^2 \left[ 2\nu_{i,s} \nu_{ii,s} \sqrt{\eta_B} \sqrt{\frac{m_e}{m_{i,s}}} (\eta_B + \eta_{ii,s} + 2 - E_{bo} - B) \right] \\ - \frac{2}{\sqrt{\pi}} e^{-\eta_c} (\eta_c + B) = 0. \end{aligned} \quad (28)$$

where

$$B = \sum_{s=1}^2 \left[ \frac{m_e}{m_{i,s}} (2 + \eta_{i,s}) + \frac{m_e}{m_{i,s}} \nu_{ii,s} (2 + \eta_{ii,s}) \right] \quad (29)$$

This equation contains three unknowns ( $\eta_c, J_b$  and  $E_{bo}$ ) for a given gas ( $\eta_{i,s}, \eta_{ii,s}$  and  $m_{i,s}$ ). Recall that  $\nu_{i,1}, \nu_{i,2}, \nu_{ii,s}$  and  $\eta_B$  are functions of  $\eta_c, J_b$  and  $E_{bo}$  only.

Improvements to the earlier model are necessary because this model grossly over-predicted the cathode temperature and therefore the thermionic emission current density for high pressure operation. In this form of the model, the ion number density was determined from the energy balance in the ionization region [9,11,12]. That is, the ion density (only singly-charged ions for a single gas type were considered) was determined by dividing the net energy available by the ionization energy until the plasma reached full ionization. Once full ionization was reached, the ion density remained constant. The heat flux for this solution increased with increasing cathode temperature and then decreased sharply once full ionization was reached. The possible solutions of the combined plasma and thermal models existed as three points, at the origin (trivial solution), on the partially ionized side of the curve (increasing heat flux with temperature), and on the fully ionized side (decreasing heat flux). However, only the trivial and fully ionized solutions are stable [11,12]. Although the results from this model were reasonable for low pressures, at higher pressures they were significantly different from the experimental data. To help correct this problem, equilibrium ionization/recombination (two-temperature Saha equation) was added to determine the species fractions in the ionization region. Molecular disassociation is not included since the disassociation temperature is much lower than the expected temperatures (0.5 to 2 eV). The general reaction rate for ionization/recombination is given for a two-temperature plasma by,

$$K_{s+1} = \frac{Y_{s+1} Y_e^\theta}{Y_s} = \frac{Z_{s+1} Z_e^\theta}{Z_s} \exp\left(\frac{\epsilon_{s+1}}{kT_h}\right) \quad (30)$$

where  $Y_s$  is the species mole fraction,  $Z_s$  is the partition function,  $\theta$  is the ratio of the electron and heavy temperatures and  $s$  ranges from 0 for the neutral to 3 for the third ion [20]. The mole fractions are defined for each gas type. For example the mole fraction of the electrons for gas type "s" is given by

$$Y_{e,s} = \frac{n_{e,s}}{n_{e,s} - \sum_{t=0}^3 n_{t,s}} \quad (31)$$

Since only monatomic heavy species are considered the partition functions for the two heavy species reduce to only the electronic component. The number of levels included is set such that the energy levels are lowered due the presence of the plasma [21].

$$\epsilon_{s+1} < \epsilon_i \left( \frac{Z_e e^2}{4\pi\epsilon_0} \left( \frac{e^2 (n_{ee} + \sum_s Z_s^2 n_s)}{2\epsilon_0 kT_e} \right)^{1/2} \right) \quad (32)$$

To decrease the numerical complexity, the energy levels were consolidated into bands [20].

Three ionization levels are considered, although only first and second levels are used in the model, to verify that the fraction of third ions is small. All species are considered as ideal gases. Note that Bose [20] recommends that  $\theta$  be less than 2 or anomalous values may be calculated. Also, Richley and Tuma recommend that the difference between  $T_e$  and  $T_h$  not exceed 2000 K for similar reasons [22]. However, some authors violate both of these recommendations and set  $T_h$  to the cathode temperature (2500 to 3700 K) while  $T_e$  is typically around 11,000 K [23]. For this study, only a single plasma temperature has been considered.

The effect of the sheath voltage on the plasma properties can be seen in Figs. Fig. (3) through Fig. (5). For a given cathode temperature, increasing the sheath voltage results in increases in both the current density and the heat flux. Also, increasing the voltage shifts the peak heat flux value to lower cathode temperatures. For the larger voltages, it can be observed that the heat flux initially increases with cathode temperature then decreases, and finally begins to increase again as heating from the doubly-charged ions becomes significant. The heat flux will continue to increase beyond this point. Solutions are only presented for a small portion of this region due to numerical difficulties with the solutions of the Saha equation with the rapidly increasing electron temperatures. In general, as the cathode temperature increases (and therefore the thermionic current increases) more energy is added to the ionization region and the electron temperature increases (all other parameters kept constant). The species number densities will increase along with the increase in electron temperature.

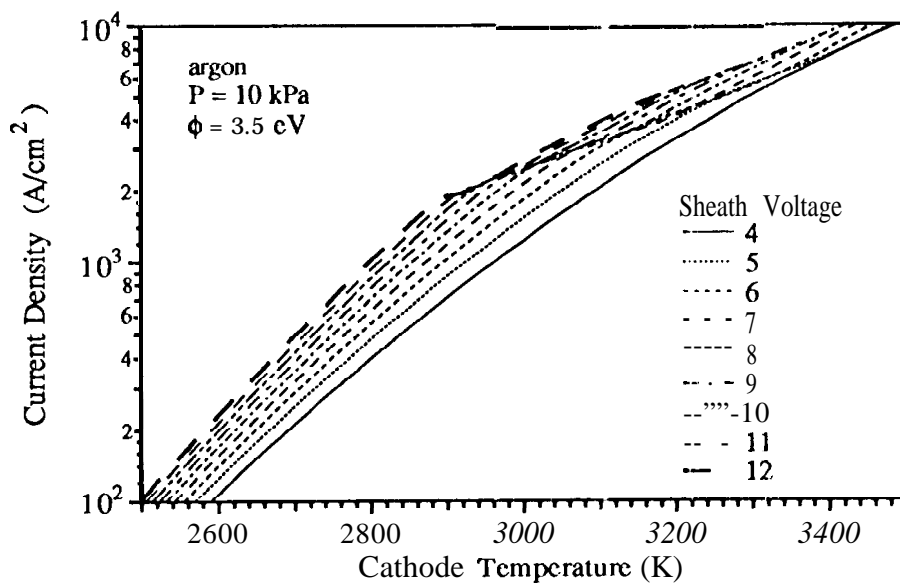


Figure 3: Current density as function of surface temperature with  $V_c$  as a parameter.

The effect of the pressure on the plasma properties can be seen in Figs. 6 through 8. A decrease

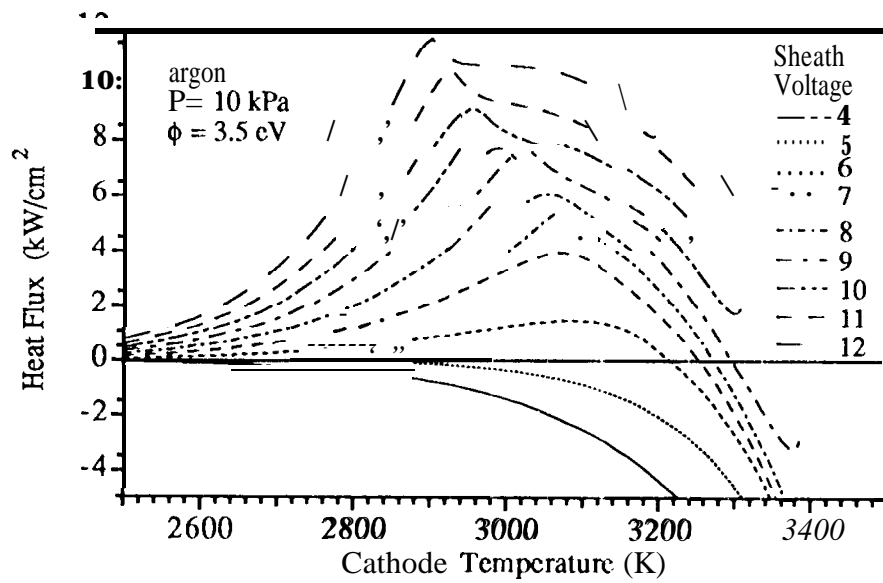


Figure 4: Heat flux as function of surface temperature with  $V_c$  as a parameter.

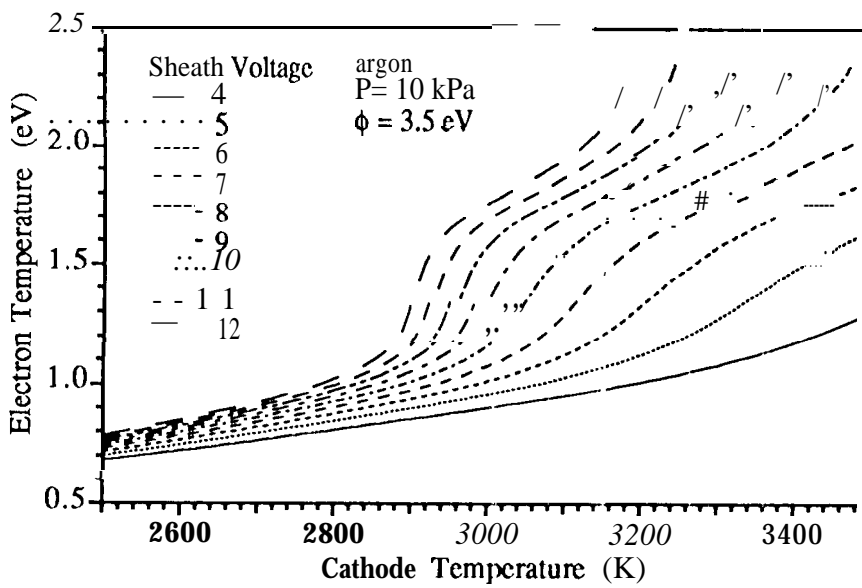


Figure 5: Electron Temperature as function of surface temperature with  $V_c$  as a parameter,

in pressure significantly shifts the zero intercept of the heat flux curves toward lower temperatures indicating that at lower pressures the cathode will operate at lower temperatures. Correspondingly the arc attachment area will increase due to a decrease in current density.

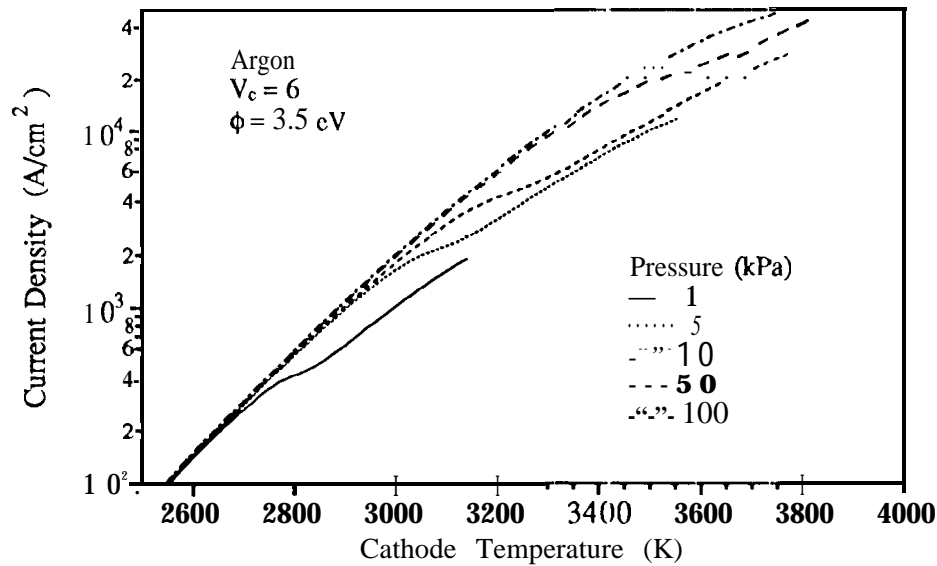


Figure 6: Current density as function of surface temperature with  $P$  as a parameter.

### Thermal Model

For a given set of boundary conditions, the thermal model describes the temperature distribution within the cathode. There are several orders of approximation by which the thermal model can be done ranging from simple one-dimensional analytical models to complex two-dimensional (axisymmetric) numerical ones [24,12,14]. Past models using the one-dimensional thermal models have assumed that the arc attachment area covered the entire tip [9,1 1,23,12], which presents two problems. First, as the surface temperature is changed, the current density will significantly change and therefore the total current will change. For high current cases this change in the total current will significantly affect the thermal model since the dominant heating mechanism is from Ohmic heating. It also makes comparing the effects of the different parameters at constant current difficult since each case produces a different total current. Second, this assumption does not correctly account for operation where the attachment area is only over a small portion of the tip, for example see Fig. (9).

For this study the two-dimensional finite-volume model used to investigate the spot heating effect at the cathode tip that could be added to the one-dimensional to create a quasi-two-dimensional model. The geometry considered is shown in Fig. (10). The variables were normalized

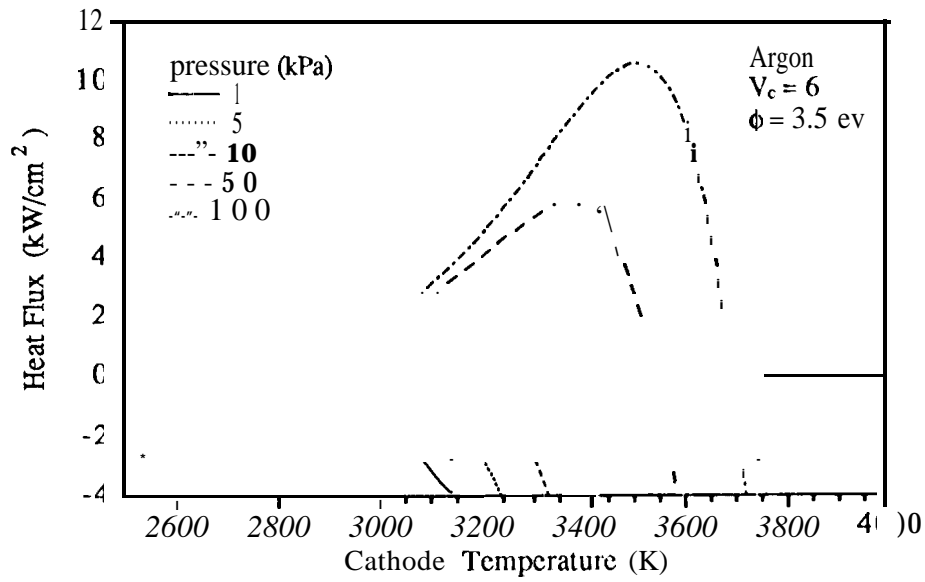


Figure 7: Heat flux as function of surface temperature with  $P$  as a parameter.

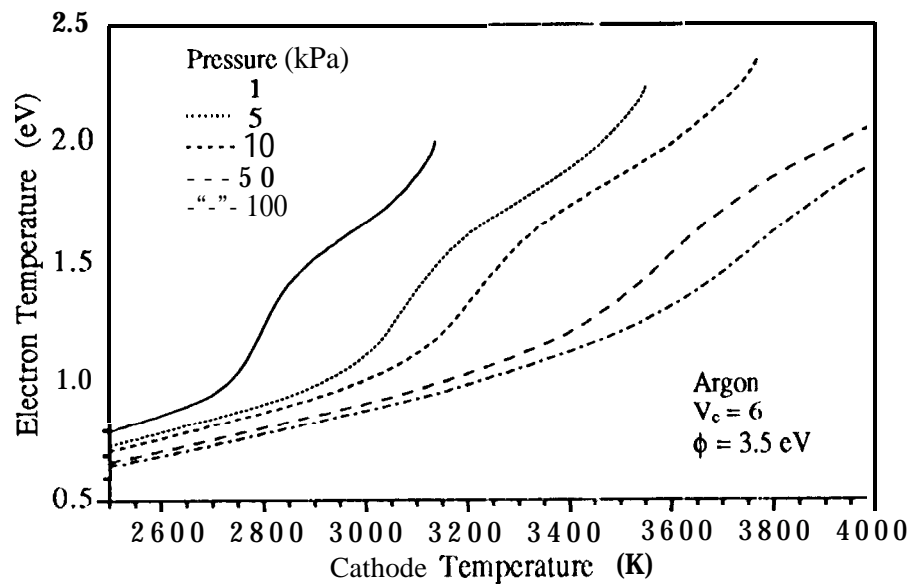


Figure 8: Electron Temperature as function of surface temperature with  $P$  as a parameter.

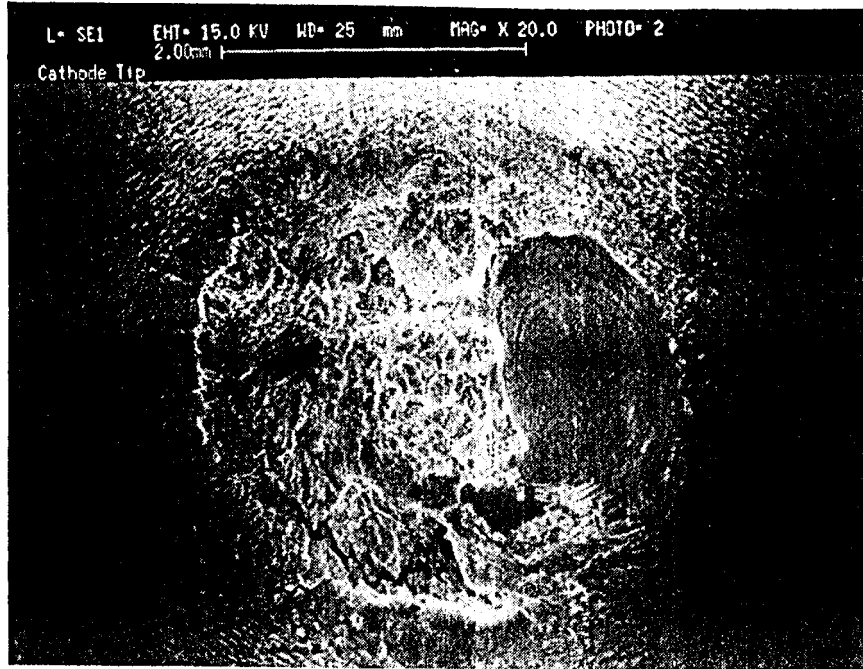


Figure 9: Photomicrograph of the eroded cathode tip from 10 kV ammonia arcjet 1470 hour test.

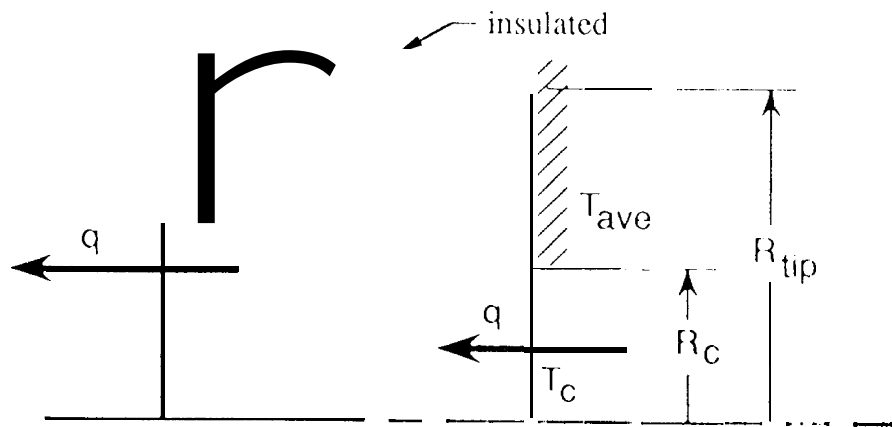


Figure 10: Two dimensional tip approximation geometry.

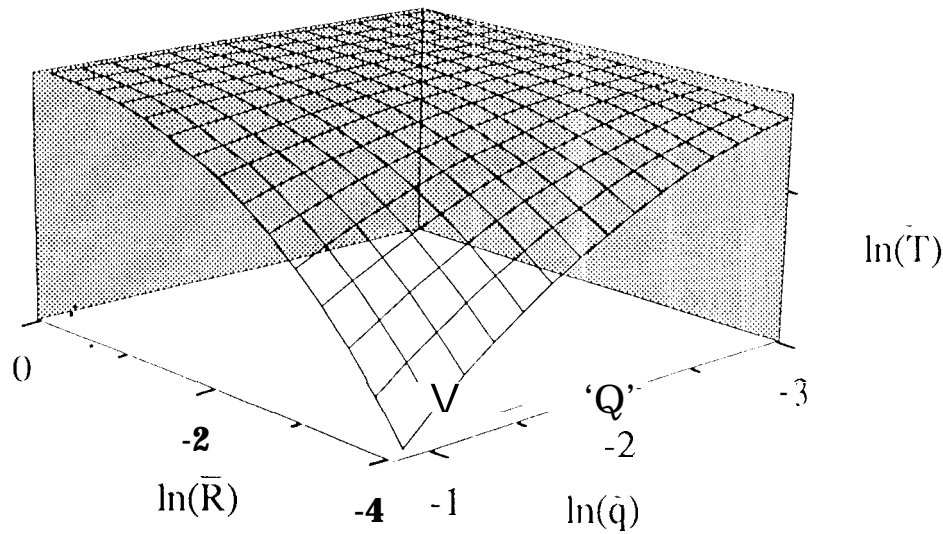


Figure 11: Two dimensional tip approximation surface fit

such that  $T = T_{ave}/T_c$ ,  $R = R_c/R_{tip}$ , and  $q = \omega/(k_{th}T_{ave}R_{tip})$  where  $T_{ave}$  is the area weighted average surface temperature,  $T_c$  is the temperature of the arc spot (assumed to be uniform),  $R_c$  is the arc spot radius,  $\omega$  is the tip radius, and  $q$  is the heat load. A series of cases were run to determine  $T$  as a function of  $R$  and  $q$ . The natural logarithms of the results were fit to a 16 parameter (constant through cubic products) surface shown in Fig. (11). A better fit was obtained in ln space than in real space. The curve fit has a maximum relative error of 1.7 percent and a maximum absolute error of 0.9 percent when converted back to real space. With this fit the spot temperature,  $T_c$ , of the plasma model is related to the average tip temperature  $T_{ave}$ , used for the thermal model for a given heat load. The attachment area is determined from the current density calculated from the plasma model and the known total current. The heat load is then determined from the heat flux calculated from the plasma model and the calculated attachment area. The final solution is obtained through an iterative process.

### Ammonia Arcjet Thruster Comparisons

The plasma model and the thermal model are combined to form the overall solution. Solutions are found where the heat flux curves for the two solutions intersect. In general there may be four possible solutions, namely, the trivial solution, two low temperature solutions, and a high temperature solution (typically around where the plasma reaches full ionization as with the previous models). The second low temperature point is a result of adding the quasi two dimensional

approximation to the thermal model described above. Both the plasma model and the thermal model solutions are shown in Fig. (12). The two intercept points shown are the two possible low temperature points but only the left (lower temperature) point is stable. That is, temperature perturbations from this point will restore the solution while for the higher temperature point a perturbation will cause the solution to move away from the point. Therefore the addition of the new approximation to the thermal model has enabled the overall model to have a stable solution on the partially ionized portion of the curve. Note that the solution point near full ionization still grossly over predicts the current density.

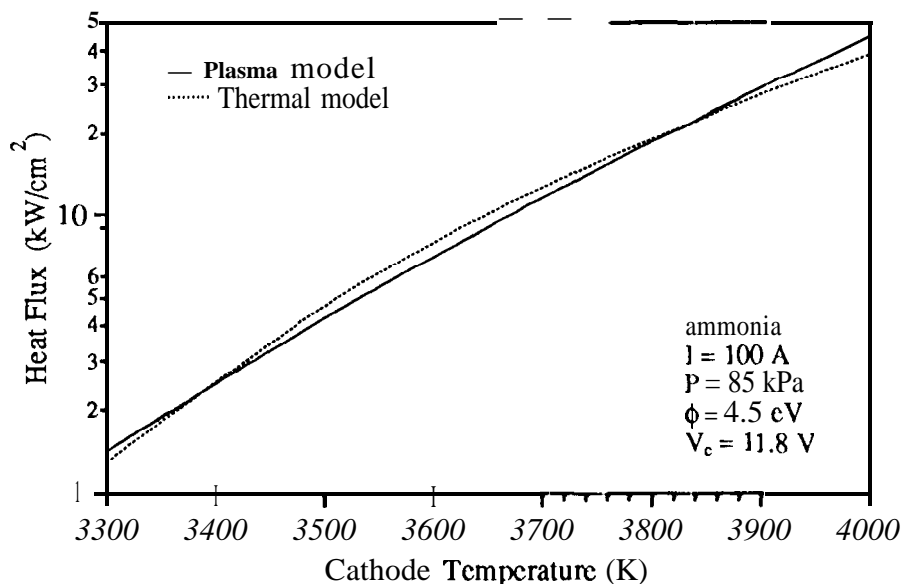


Figure 12: Heat flux as a function of cathode temperature for a  $V_c$  value of 11.8 V.

Comparisons between the model and 10 kW and 25 kW ammonia arcjet long duration test data with thoriated tungsten cathodes are presented. A plot of the sheath voltage versus cathode temperature for both cases is shown in Fig. (13) and predicted electron temperatures are shown in Fig. (14). There are two possible solutions for a given sheath voltage corresponding to the two intercepts in Fig. (12). The peak value occurs when only one intercept point exists and it is only marginally stable. The stable points are to the left of the maximum point. The slight step in the curve left of the maximum point occurs at the point where the attachment area equals the tip area, and is a result of limitations of the quasi-two-dimensional approximation surface fit at this point. For cases left of this point, the attachment area will be larger than the tip area. The model assumes for these cases that an "enlarged" tip area equal to the attachment area exists at a uniform temperature,  $T_c$ .

The attachment area as a function of cathode temperature is presented in Fig. (15) for the 10 kW case and in Fig. (16) for the 25 kW case. The horizontal lines represent physical areas for

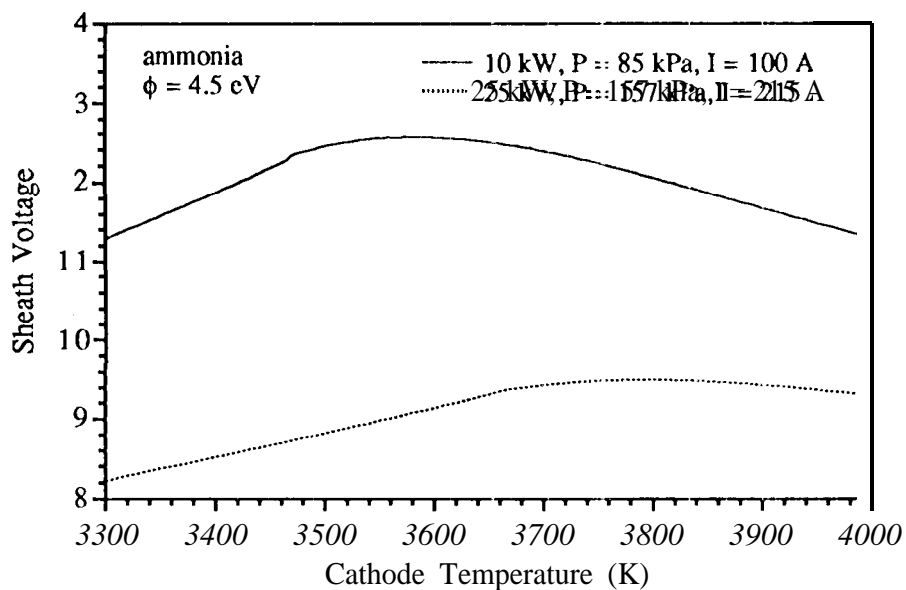


Figure 13: Sheath Voltage as a function of cathode temperature for 10 kW and 30 kW ammonia arcjets.

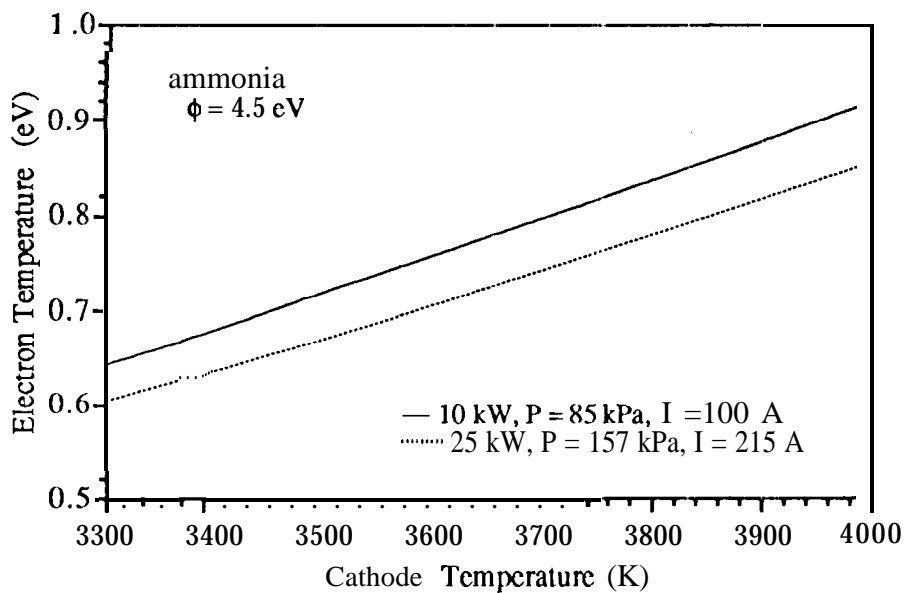


Figure 14: Electron temperature as a function of cathode temperature for 10 kW and 30 kW ammonia arcjets.

each cathode tip. For the 10 kW case, the lower line represents the size of the molten oval spot shown in Fig. (9) [25]. Materials analysis of this cathode after testing showed that was molten prior to shut-down [25] so that the actual operating temperature would be around 3660 K. A surface work function of 4.5 eV for pure tungsten, is used in the model since analysis of the molten spot revealed no traces of thorium. The model predicts a cathode temperature of 3670 K for an attachment area equal to that of the molten spot. Although the model appears to agree well with the experimental data, this point falls on the unstable side of the voltage curve. The closest stable point would be near the peak voltage point. The temperature of the peak voltage point or maximum stable point is about 3585 K for the 10 kW case and about 3790 K for the 25 kW case. For the 25 kW case it is less obvious from the experimental data what size the attachment area was at shut-down, A cross-section of the cathode tip after testing is shown in Fig. (17) [26]. The severe erosion for the case indicates that a significant portion of the tip was molten. The horizontal line in Fig. (16) represent the areas associated with the entire hemispherical surface ( $2\pi R_c^2$ ) and the cross-sectional area at tile opening ( $\pi R_c^2$ ) where  $R_c$  is the crater radius. The actual attachment area probably is between these two extremes, For this case the molten temperature point falls on the stable side of the curve and with an area just larger than the cross-sectional area suggesting that, the model agrees well with the data.

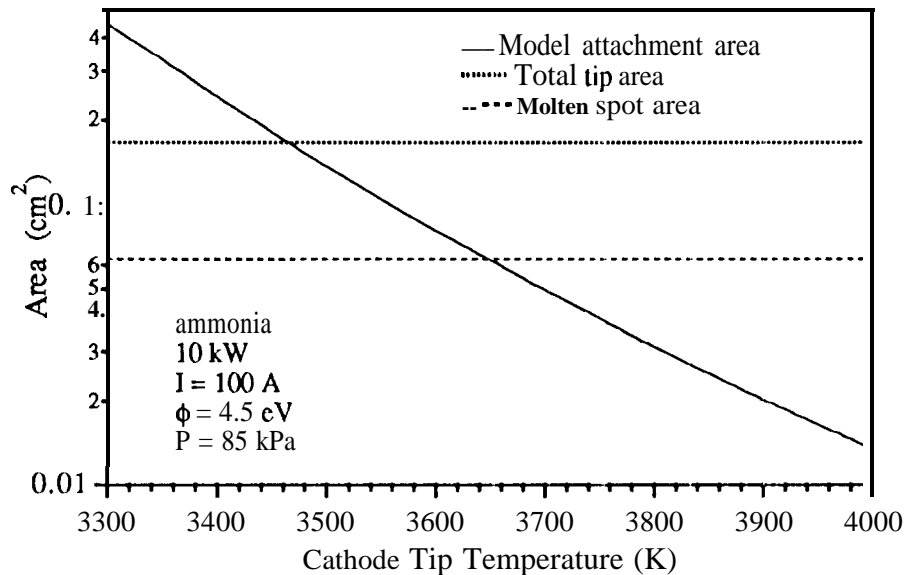


Figure 15: Attachment area as a function of cathode temperature for a 10 kW ammonia arcjet.

### Conclusions

Additions to the plasma model to include doubly-charged ions, equilibrium ionization/recombination were made to determine species densities, and the ability to model gas mixtures. The addition of a

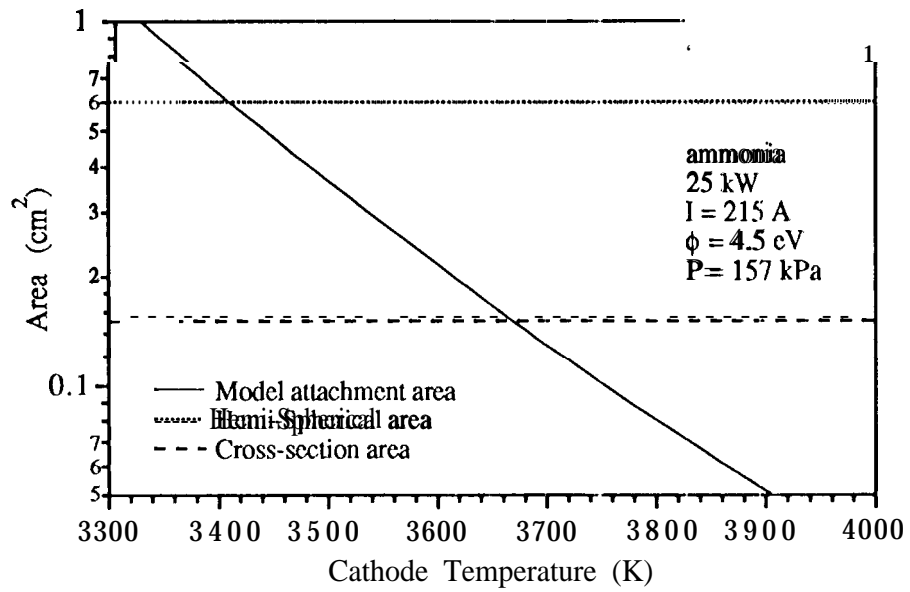


Figure 16: Attachment area as a function of cathode temperature for a 30 kW ammonia arcjet.



Figure 17: Photograph of cross-section of the eroded cathode tip from 30 kW ammonia arcjet 573 hour test.

quasi-two-dimensional model approximation to the thermal model allows the use of arc attachment areas smaller than the total tip area. Since the attachment area is now alterable, cases for constant total current can be compared. Also, this addition provides a stable low temperature solution that agrees well with the experimental data. Recently, excellent agreement between the new model and high-power long-duration ammonia arcjet data was achieved for the 25 kW case; although, the model slightly underpredicts the cathode temperature for the 10 kW case. Likewise, post-test analysis of arcjet cathodes indicates that portions of the cathode tip were molten during operation. Concurrently, the model predicts temperatures near the melting point of tungsten for attachment areas consistent with the areas observed in the experiments.

### Acknowledgements

The research described in this paper was conducted at the Jet Propulsion Laboratory, California Institute of Technology under contract with the National Aeronautics and Space Administration.

### List of Variables with typical units

$a$	constant
$A$	area ( $\text{m}^2$ )
$A_R$	Richardson coefficient ( $\text{A}/\text{m}^2/\text{K}^2$ )
$B$ or $C$	Constant
$d$	ionization region thickness (m)
$e$	electron charge (C)
$E$	electric field (V/m)
$E_{b,o}$	Normalized thermionic electron thermal energy
$F$	particle flux (particle/s)
$I$	total current (A)
$j$	current density ( $\text{A}/\text{m}^2$ )
$J_b$	normalized thermionic current density
$k$	Boltzman constant (J/K)
$k_{th}$	thermal conductivity (W/m/K)
$K$	equilibrium reaction rate
$L$	characteristic length (m)
$m$	particle mass (kg)
$n$	number density ( $\text{particle}/\text{m}^3$ )
$\dot{n}$	number density generation rate ( $\text{particle}/\text{m}^3/\text{s}$ )
$P$	pressure (Pa)
$q$	heat flux ( $\text{W}/\text{m}^2$ )
$r$	radius (m)
$R_c$	radius of arc attachment spot (m)
$T$	temperature (K)
$V$	voltage (V)
$Y$	mole fraction

$z$	position from cathode tip (m)
$Z$	partition function
$\beta$	ratio of partial pressures
$\epsilon$	normalized electric field
$\epsilon_i$	ionization energy (eV)
$\epsilon_0$	permittivity of free space ( $C^2/N/m^2$ )
$\eta$	normalized voltage
$\eta_i$	normalized ionization energy
$\nu_i$	normalized ion density at sheath edge
$\eta_B$	normalized Bohm energy
$\phi$	work function (eV)
$e$	normalized temperature or ratio of electron to heavy temperature
subscripts	
b	thermionic (beam) electron
B	Bohm energy value
c	cathode surface
e	plasma electron
eff	effective
ei	electron-ion collision
h	heavy particle (neutral or ion)
i	singly-charged ion
ii	singly-charged ion
n	neutral
p	main plasma
o	reference value
s	gas type ( $s = 1$ or $2$ )
Sh	sheath edge
tot	total

## References

- [1] J. E. Polk, A. J. Kelly, and R. G. Jahn. Mechanisms of Hot Cathode Erosion in MPD Thrusters. In *21st International Electric Propulsion Conference*, Orlando, FL, 1990. AIAA-90-2673.
- [2] P. H. Prewett and J. E. Allen. The Double Sheath Associated with a Hot Cathode. *Proceedings of the Royal Society of London*, 348:435-446, 1976.
- [3] D. E. Siegfried and P. J. Wilbur. A Model for Mercury Orificed Hollow Cathodes: Theory and Experiment. *AIAA Journal*, 22(10):1405-1412, 1984.
- [4] K. D. Goodfellow and S. N. B. Murthy. Electrode Irrecesses and MPD Thruster Operation. In *24th Joint Propulsion Conference*, Boston, MA, 1988. AIAA-88-3207.

- [5] A. Salhi and P. J. Turchi. A First-Principles Model for Orificed Hollow Cathode Operation. in *28<sup>th</sup> Joint Propulsion Conference*, Nashville, TN, 1992. AIAA 92-3742.
- [6] K. Kuwahara and et. al. Thermal Characteristics of MPD Arcjet. In *17<sup>th</sup> International Electric Propulsion Conference*, Tokyo, Japan, 1984, IEPC 8459.
- [7] R. C. Mehta. Thermal Analysis of a Conical Cathode of an MPD Arc, *AIAA Journal*, 17(11):1272-1274, 1979.
- [8] J. Weng and E. J. Seldin. Calculation of Steady State Temperatures in Graphite electrodes in an Electric Arc Steel Furnace. *Carbon*, 15:391-398, 1977.
- [9] W. L. Bade and J. M. Yes. Arcjet Technology Research and Development-Final Report. Technical Report NASA CR-54687, AVCO Corporation, Wilmington, MA, 1965.
- [10] D. Q. King. Feasibility of Steady-State Multi-Megawatt MPD Thrusters. In *18<sup>th</sup> International Electric Propulsion Conference*, Alexandria, VA, 1985. AIAA 85-2004.
- [11] K. D. Goodfellow, T. J. Pivrotto, and J. E. Polk. Applied-Field Magnetoplasma Dynamic Engine Developments. in *28<sup>th</sup> Joint Electric Propulsion Conference*, Nashville, TN, 1992. AIAA 92-3293.
- [12] K. D. Goodfellow and J. E. Polk, High Current Cathode Thermal Behavior, Part I: Theory. In *23rd International Electric Propulsion Conference*, Seattle, WA, 1993. IEPC 93-030.
- [13] K. D. Goodfellow and J. E. Polk. Experimental Verification of a High-Current Cathode Model. In *31<sup>th</sup> Joint Electric Propulsion Conference*, San Diego, CA, 1995. AIAA 95-3062.
- [14] K. D. Goodfellow and J. E. Polk. Theoretical Operation of Solid Rod Cathodes. In *30<sup>th</sup> Joint Propulsion Conference*, Indianapolis, IN, 1994. AIAA 94-3132.
- [15] W. Neumann. *The Mechanism of the Thermoemitting Arc Cathode*. Akademie-Verlag Press, Berlin, Germany, 1987.
- [16] D. Bohm. *The Characteristics of Electrical Discharges in Magnetic Plasma*. McGraw-Hill, New York, 1949.
- [17] F. F. Chen. *Introduction to Plasma Physics and Controlled Fusion, Vol. 1, Plasma Physics*, 2nd ed. Plenum Press Book Co., New York, 1984.
- [18] J. G. Andrews and J. E. Allen. Theory of a Double Sheath Between Two Plasmas. *Proceedings of the Royal Society of London*, 320:459-472, 1971.
- [19] M. Mitchner and C. H. Krugar. *Partially Ionized Gases*. John Wiley and Sons, New York, 1973.
- [20] T. K. Bose. Thermophysical and Transport Properties of Multi-Component Gas Plasmas at Multiple Temperatures. *Progress in Aerospace Sciences*, 25:1-42, 1987.

- [21] B. R. Griem. *Plasma Spectroscopy*. McGraw-Hill Book Co., New York, 1964.
- [22] E. Richley and D. T. Tuma. On the Determination of Particle Concentrations in Multitemperature Plasmas. *Journal of Applied Physics*, 53(12):8537-8542, 1982.
- [23] X. Zhou, D. Berns, and J. Heberlein. Investigation of Arc-Cathode Interaction. In *30<sup>th</sup> Joint Propulsion Conference*, Indianapolis, IN, 1994. AIAA 94-3129.
- [24] F. P. Incropera and D. P. DeWitt. *Fundamentals of Heat Transfer*. John Wiley and Sons, New York, 1981.
- [25] K. D. Goodfellow and J. E. Polk. Ammonia Arcjet Experiments in Support of the ELITE Flight Experiment. JPL internal document, 1993. JPL D-11268.
- [26] T. J. Pivrotto and W. D. Deininger. High Current Cathode Thermal Behavior, Part 1: Theory. in *20<sup>th</sup> International Electric Propulsion Conference*, Garmisch-Partenkirchen, W. Germany, 1988. IEPC 88-074.